Combustion and Flame 272 (2025) 113901

Contents lists available at ScienceDirect

Combustion and Flame

journal homepage: www.sciencedirect.com/journal/combustion-and-flame

Adjoint-based mean-flow uncertainty and feedback-forcing analyses of a thermoacoustic model system

Jiasen Wei *, Alessandro Bottaro, Jan O. Pralits

DICCA, Università degli Studi di Genova, via Montallegro 1, Genova, 16145, Italy

ARTICLE INFO

Keywords:
Thermoacoustic systems
Adjoint approach
Sensitivity analysis
Uncertainty quantification

ABSTRACT

Clean combustion, particularly premixed hydrogen combustion aimed at reducing NOx emissions, is prone to thermoacoustic instabilities that can cause structural vibrations and equipment failures. This study focuses on a low-order model for a thermoacoustic prototype, a simple quasi-one-dimensional combustor comprising a plenum, premixing duct, and combustion chamber. Resonant modes of the combustor are identified by solving a nonlinear eigenvalue problem. Using an adjoint-based sensitivity analysis, the impact of uncertainties in base flow parameters on resonant frequencies and linear growth rates is assessed. The results obtained highlight the significant influence of variations in cold gas density within the plenum and premixing duct on the linear growth rates, potentially explaining discrepancies with literature data. Additionally, structural sensitivities in both the base and the perturbation flow are examined to evaluate the effects of a generic feedback mechanism on the eigenvalues. Structural sensitivities at the base-flow level are evaluated as a function of the flame position, identifying effective stabilizing mechanisms such as heat addition and mass flow rate reduction at duct intersections. The most stabilizing feedback mechanism is identified as mass fluctuations proportional to pressure perturbation at the end of the plenum, an effect achievable with Helmholtz resonators. Adjoint analyses permit uncertainty quantification of base-state parameters and gradient information for optimization strategies aimed at mitigating thermoacoustic instabilities through efficient and low-cost calculations.

Novelty and significance statement

The novelty of this research lies in its development of a comprehensive adjoint analysis framework for three types of sensitivity analyses within a thermoacoustic premixed combustor model. This paper uses base-state sensitivity to quantify the significant effect of base flow uncertainties, such as cold gas properties in the premixer, on the unstable resonant mode growth rates. In addition to structural perturbation sensitivity analysis, it uniquely applies structural sensitivity to base flow modifications, uncovering effective steady control mechanisms like mass suction and heating. The findings identify efficient approaches to mitigate thermoacoustic instabilities in premixed combustion systems and broaden the scope of potential control strategies.

1. Introduction

Thermoacoustic instabilities are self-excited oscillations that arise when pressure oscillations are coupled with heat-release oscillations. If the pressure oscillations are in phase with the unsteady heat release rate, instabilities might emerge, causing unwanted consequences that range from annoying noise to catastrophic structural damage [1]. These phenomena are of paramount importance in various industrial apparatuses such as gas turbines, rockets, and domestic gas boilers.

Considerable research has been dedicated to modeling and predicting thermoacoustic instabilities both in laboratory setups and industrial equipment. A thorough summary of the mechanisms of combustion instabilities and common methods of analysis has been published by Culick [2] and Raun et al. [3]. Galerkin techniques have been used extensively to model combustion instabilities. Balasubramanian and Sujith [4] used the Galerkin technique to analyze the acoustic pressure oscillations and ensuing nonlinear dynamics in a Rijke tube. A drawback of this approach is that the acoustic flow variables (usually pressure or acoustic velocity oscillations) are represented as a modal Galerkin expansion, a sum of infinite series. In practice, the result must be truncated while the discontinuity in the velocity at the compact heater location needs proper resolution; this might lead to spurious oscillations arising from the Gibbs phenomenon [5,6]. Sayadi et al. [6]

* Corresponding author.
E-mail address: jiasen.wei@edu.unige.it (J. Wei).

https://doi.org/10.1016/j.combustflame.2024.113901
Received 11 August 2024; Received in revised form 2 December 2024; Accepted 2 December 2024
Available online 12 December 2024

highlight clearly the limitations of three different Galerkin approaches (which use the continuous acoustic modes of the chamber, without the heater, as basis functions), and recommend special attention when adopting the Galerkin method to study thermoacoustic systems with discontinuous terms.

Another widely-used modeling approach is the wave-based approach, initially described by Rayleigh [7]. The Riemann invariants are used to decompose the flow fluctuations into upstream- and downstream-traveling components. Crocco and Cheng [8] employed a wave-based approach to analyze the high-frequency oscillations in a rocket combustion chamber. This method was later extended to full acoustic networks by Dowling [5]. With the network modeling approach, the geometry, boundary conditions, and heat-release source of the combustion system are modeled as individual elements, each described by a linear transfer function, connected by jump conditions. The method was adapted by Schaefer and Polifke [9] to treat systems with duct elements of varying cross-sectional area and arbitrary mean temperature profiles. Evesque and Polifke [10] applied the wave-based modeling approach to a generic annular combustor and investigated the effect of non-identical burners as a means of passive control. Ghirardo et al. [11] focused on can-annular combustors in the low-frequency range, showing that the connection between neighboring cans may trigger azimuthally-traveling unstable modes.

Identifying possible passive control strategies to suppress thermoacoustic instabilities can be done efficiently by conducting sensitivity analyses. The adjoint method is a powerful tool for solving stability, receptivity, sensitivity, and control problems in complex systems, with extensive applications in hydrodynamics stability [12–14]. Previous adjoint-sensitivity work can be broadly subdivided into three types of analysis.

- To evaluate eigenvalue variations due to generic base-state modifications δU, possibly related to uncertainties in the measurement or in the calculation of the base state. Bottaro et al. [15] first applied the *base-state sensitivity analysis* to examine the eigenvalues of the Orr–Sommerfeld operator. They found variations (of given amplitude) of the basic flow with the most destabilizing effect on the eigenvalues for the case of the plane Couette flow and introduced the concept of the δU-pseudospectrum.
- To find the eigenvalue changes due to feedback sources in the flow disturbances. This is often referred to as *structural sensitivity analysis*. Giannetti and Luchini [16] conducted such an analysis for the case of the flow around a cylinder and identified regions in which variations, for instance, due to truncation of the domain or grid resolution, cause the largest eigenvalue drift.
- To evaluate the sensitivity of source terms acting on the steady equations of the base flow in order to stabilize unstable eigenmodes. Marquet et al. [17] calculated the *sensitivity to a steady force* and gave predictions of possible passive control methods to suppress the vortex shedding in the wake of a cylinder. Pralits et al. [18] introduced the idea of *structural sensitivity to base-flow modifications* and showed successful examples of its application. Other steady source terms can easily be envisaged, for the mass and/or energy conservation equations. Luchini et al. [19] conducted a structural sensitivity analysis for finite-amplitude global modes on a periodic base flow and showed good comparison with experiments on the flow control in the cylinder wake.

Existing literature reflects substantial endeavors towards uncertainty quantification and sensitivity analysis in thermoacoustic systems [20,21]. A comprehensive review of the applications of adjoints to thermoacoustic problems has been published by Magri [22]. Compared with the traditional finite-difference approach, the adjoint method is more cost-effective in the analysis of systems that depend on many parameters. An example of the use of these two approaches will be shown later on.

Adjoint sensitivity analysis has also been used in shape optimization of thermoacoustic systems such as the Rijke tube, in swirl combustors [23], also using low-order models [24–26]. Mensah and Moeck [27] applied the adjoint perturbation theory to a generic annular combustor model and found the optimal damper arrangements and the impedance design to mitigate instabilities. Magri et al. [28] applied the adjoint analysis to calculate the first variation of the Rayleigh criterion in both the time and frequency domains. They also proposed an adjoint Rayleigh criterion, which reflects the effect of unsteady heat release rate on the first variation of eigenvalues. Schäfer et al. [29] developed a hybrid adjoint approach, exploiting the self-adjointness of duct element and simplifying the derivation of adjoint system, for sensitivity analysis of thermoacoustic network models. By computing the feedback sensitivity and base-state sensitivity of an annular combustor network model, they tuned a Helmholtz resonator to achieve passive control. Juniper [30] developed a pedagogical framework of adjoint Helmholtz solvers and calculated receptivity, feedback sensitivity, and base-state sensitivity for a Rijke tube and a rocket engine combustor model. Base-state sensitivities were calculated to evaluate the effect of variables such as the time delay in the heat release model, the boundary conditions, and the heat release distribution. Aguilar et al. [25] calculated feedback sensitivity and base-state sensitivities of reflection coefficients, time delay, and interaction index of the heat release model in a one-dimensional two-segment thermoacoustic system. In a later study, Aguilar and Juniper [26] optimized the combustor geometry based on the sensitivity analysis of a longitudinal bluff-body combustor. They examined the eigenvalue variation due to the steady base flow alteration by changing the combustor geometry. This is similar to the third type of sensitivity analysis mentioned above, but not quite the same, because there is no steady force introduced into the system. To the authors' best knowledge, the use of adjoint-based sensitivity analysis to identify steady forcings to base flow equations that stabilize thermoacoustic systems has yet to be carried out.

Existing feedback control techniques and devices have been extensively studied. Raghu and Sreenivasan [31] examined a set of active control methods, including heat addition, force addition, and periodic mass addition, for the suppression of pressure oscillations in a laboratory scale pipe flow and demonstrated that the combination of mesh screens and heating coils applied to a large combustion set-up successfully eliminated undesired pressure oscillations. Dowling and Morgans [32] summarized the application of feedback control to mitigate thermoacoustic instabilities, including the development of control strategies and controller design. They also demonstrated a case of feedback control on a full-scale combustion system. Another thorough review by Zhao and Li [33] described the use and effectiveness of acoustic dampers in aerospace combustors. Zhao and Morgans [34] used Helmholtz resonators with tuned geometry to stabilize combustion systems with multiple unstable modes, validated through numerical simulations and experiments on a Rijke tube.

The aim of this paper is to show, for a prototypical thermoacoustic system, the application of all three types of adjoint analysis alluded to above, for the assessment of uncertainties and the identification of passive control strategies. The structure of the present contribution is as follows: in Section 2, details of the lumped model of the combustor by Dowling and Stow [35] are given. Linear stability analysis yields the eigenspectrum, highlighting some discrepancies with the literature, particularly with respect to the amplification rate of the eigenmodes. In Section 3, we investigate the reasons for these discrepancies, relating them to base-flow uncertainties by applying the adjoint base-state sensitivity analysis. In Sections 4 and 5, we aim to find optimal control strategies to mitigate thermoacoustic instabilities with a focus on the two most unstable eigenmodes. In Section 4, the sensitivity to structural modifications in the base flow is evaluated against variations in the flame position within the combustor. In Section 5, we apply the structural sensitivity analysis to evaluate the eigenvalue drift due to feedback forcings in the disturbance field. Section 6 presents the main conclusions of the work.

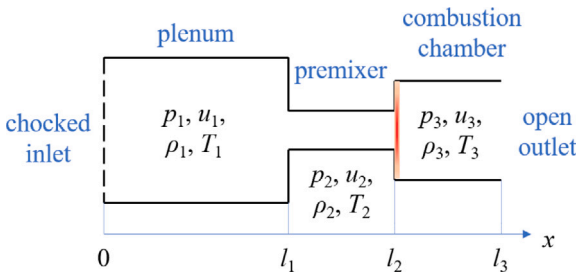

Fig. 1. Sketch (not-to-scale) of the one-dimensional three-duct combustor geometry, with notations and boundary conditions. The positions of the ducts' intersections are $x = l_1$ and $x = l_2$ (where the compact flame is also located); the outlet of the system is at $x = l_3$.

Table 1
Geometrical parameters of the three-duct combustor.

Section	Length		Cross-sectional area	
Plenum	L_1	1.7 m	a_1	0.0129 m^2
Premixer	L_2	0.0345 m	a_2	0.00142 m^2
Combustion chamber	L_3	1.0 m	a_3	0.00385 m^2

2. The one-dimensional premixed combustion system

2.1. General description

The prototypical thermoacoustic system examined in this work is the quasi-one-dimensional combustor reported in Dowling and Stow [35], displayed in Fig. 1. The simplified combustor geometry is based on the assumption of sufficiently low oscillation frequencies in the combustor so that radial modes are cut off, and only plane waves transport acoustic energy.

The system consists of a plenum, a premix duct, and a combustion chamber, modeled as three straight ducts connected by discontinuities where jump conditions must be enforced. The area changes, and the unsteady heat source (modeling the flame) are short enough to be considered acoustically compact. The compact flame is located at the outlet of the premixer. The combustor has a choked inlet to model the flow supplied by a centrifugal blower and an open outlet as the burned gases are discharged into an open space or another large plenum. The dimensions of the system are given in Table 1.

2.2. The low-order modeling approach

The simple combustion system in Fig. 1 is treated with the lumped approach described by Dowling and Stow [35]. The flow is described by a set of equations, including governing equations, boundary conditions, and jump conditions, with the ideal gas assumption. The equations are linearized around the base flow; thus, in each duct, the flow variables are decomposed into a mean steady value plus a perturbation, viz. $p(x,t) = \bar{p} + p'(x,t)$, $u(x,t) = \bar{u} + u'(x,t)$, $\rho(x,t) = \bar{\rho} + \rho'(x,t)$, $T(x,t) = \bar{T} + T'(x,t)$, $Q(x,t) = \bar{Q} + Q'(x,t)$, where Q is the heat release rate generated by the flame. The base flow parameters, denoted as $\bar{\mathbf{q}} = (\bar{\rho}_j, \bar{u}_j, \bar{p}_j, \bar{T}_j, \bar{Q})$, are considered uniform and steady in each duct. The independent perturbation variables are denoted as $\mathbf{q}' = (\rho'_j, u'_j, p'_j)$ with $j = 1, 2, 3$ representing each duct.

In the combustion chamber section, the mean temperature is the same as the flame temperature T_f, and the mean pressure is the ambient pressure. At the area-increasing intersection, $x = l_2$, the Borda–Carnot equation is used; at the sudden contraction in $x = l_1$, the flow is assumed to behave isentropically. The set of equations used to find the base state, $\mathbf{B}(\bar{\mathbf{q}}) = 0$, is given in Supplementary Material Part A.

In each section of the system (denoted by $j = 1, 2, 3$), the perturbations are governed by differential equations representing the conservation of mass, momentum, and energy:

$$\frac{\partial \rho'_j}{\partial t} + \bar{u}_j \frac{\partial \rho'_j}{\partial x} + \bar{\rho}_j \frac{\partial u'_j}{\partial x} = 0, \tag{1a}$$

$$\bar{\rho}_j \frac{\partial u'_j}{\partial t} + \bar{\rho}_j \bar{u}_j \frac{\partial u'_j}{\partial x} + \frac{\partial p'_j}{\partial x} = 0, \tag{1b}$$

$$\frac{\partial p'_j}{\partial t} + \bar{u}_j \frac{\partial p'_j}{\partial x} + \gamma \bar{p}_j \frac{\partial u'_j}{\partial x} = 0. \tag{1c}$$

In the system above no summation is intended over the j index. A wave decomposition is introduced for the perturbation variables; pressure, density, and velocity fluctuations in the frequency domain ($\mathbf{q}'(x,t) = \hat{\mathbf{q}}(x)e^{i\omega t}$) are decoupled as forward and backward traveling acoustic waves plus an entropy wave convected by the mean flow:

$$\hat{p}_j = A_{+j} e^{ik_{+j}x} + A_{-j} e^{ik_{-j}x}, \tag{2a}$$

$$\hat{\rho}_j = \frac{1}{\bar{c}_j^2} A_{+j} e^{ik_{+j}x} + \frac{1}{\bar{c}_j^2} A_{-j} e^{ik_{-j}x} - \frac{1}{\bar{c}_j^2} A_{ej} e^{ik_{0j}x}, \tag{2b}$$

$$\hat{u}_j = -\frac{k_{+j}}{\bar{\rho}_j \alpha_{+j}} A_{+j} e^{ik_{+j}x} - \frac{k_{-j}}{\bar{\rho}_j \alpha_{-j}} A_{-j} e^{ik_{-j}x}, \tag{2c}$$

where $k_{\pm j} = -\dfrac{\omega}{\bar{u}_j \pm \bar{c}_j}$, $k_{0j} = -\dfrac{\omega}{\bar{u}_j}$, and $\alpha_{\pm j} = \omega + \bar{u}_j k_{\pm j}$.

At the area decreasing intersection, the flow can be assumed as isentropic. With mass and energy conservation equations, the jump conditions at $x = l_1$ read

$$a_1 \left(\bar{\rho}_1 \hat{u}_1 + \hat{\rho}_1 \bar{u}_1\right) = a_2 \left(\bar{\rho}_2 \hat{u}_2 + \hat{\rho}_2 \bar{u}_2\right), \tag{3a}$$

$$\gamma \frac{\hat{p}_1}{\bar{p}_1} - \frac{\hat{\rho}_1}{\bar{\rho}_1} = \gamma \frac{\hat{p}_2}{\bar{p}_2} - \frac{\hat{\rho}_2}{\bar{\rho}_2}, \tag{3b}$$

$$\hat{H}_1 = C_p \hat{T}_1 + \bar{u}_1 \hat{u}_1 = \hat{H}_2 = C_p \hat{T}_2 + \bar{u}_2 \hat{u}_2, \tag{3c}$$

where $H = C_p T + \frac{1}{2}u^2$ is the stagnation enthalpy per unit mass and C_p the specific heat at constant pressure, assumed constant. The specific heat ratio is denoted by $\gamma = C_p/C_v$.

At $x = l_2$, where the area increases, the mass, energy, and momentum conservation apply:

$$a_2 \left(\bar{\rho}_2 \hat{u}_2 + \hat{\rho}_2 \bar{u}_2\right) = a_3 \left(\bar{\rho}_3 \hat{u}_3 + \hat{\rho}_3 \bar{u}_3\right), \tag{4a}$$

$$a_2 \hat{\rho}_2 \bar{u}_2^2 + 2a_2 \bar{\rho}_2 \bar{u}_2 \hat{u}_2 = a_3 \left(\hat{p}_3 - \hat{p}_2\right) + a_3 \hat{\rho}_3 \bar{u}_3^2 + 2a_3 \bar{\rho}_3 \bar{u}_3 \hat{u}_3, \tag{4b}$$

$$a_2 \left(\bar{\rho}_2 \bar{u}_2 \hat{H}_2 + \bar{\rho}_2 \hat{u}_2 \bar{H}_2 + \hat{\rho}_2 \bar{u}_2 \bar{H}_2\right) = a_3 \left(\bar{\rho}_3 \bar{u}_3 \hat{H}_3 + \bar{\rho}_3 \bar{H}_3 \hat{u}_3 + \bar{u}_3 \bar{H}_3 \hat{\rho}_3 - \hat{Q}\right). \tag{4c}$$

Note that the heat released by the compact flame is introduced in the jump condition. This might differ from what Dowling and Stow [35] did, since it is not clear from their paper whether the area change, from a_2 to a_3, and the energy source term Q were treated in one step (at the $x = l_2$ interface) or in two successive steps. In any event, we have modeled the problem in two ways: one is the fully coupled approach embodied by Eqs. (4) above, and the second considers two steps (and two separate sets of equations) with the area change first, and the heat release term immediately downstream. The results of the two models are close to one another, and also close to those by Dowling and Stow [35], but not identical. We have thus decided to maintain only the fully coupled approach above.

The fluctuating heat release rate generated by an unsteady flame is governed by a time-delayed model correlated with the mass flow rate in the premixer section:

$$\hat{Q} = -\kappa \bar{Q} \frac{\hat{\dot{m}}_2}{\bar{\dot{m}}_2} e^{-i\omega\tau}, \tag{5}$$

where $\tau = 0.006$ s is the time delay, and the coefficient κ acts as an unsteady flame switcher, with its value ranging from 0 to 1 [35].

Choked inlets usually model a compressor exit, where the mass and energy flow rates are nearly constant. An open outlet can be approximated with a zero-pressure oscillation. Hence, the boundary

conditions are:

Choked inlet [36]:

$$\frac{\hat{p}_1(0)}{\bar{\rho}_1} + \frac{\hat{u}_1(0)}{\bar{u}_1} = 0, \tag{6a}$$

$$\hat{p}_1(0) = \bar{c}_1^2 \hat{\rho}_1(0), \tag{6b}$$

Open outlet:

$$\hat{p}_3(l_3) = 0. \tag{7}$$

Eqs. (3)–(7) form the direct system of perturbation flow in the combustor. From the equation of state of ideal gases, with R_g the perfect gas constant, the first-order linearization of $\hat{T}$ yields

$$\hat{T} = \frac{\hat{p}/R_g - \bar{T}\hat{\rho}}{\bar{\rho}}, \tag{8}$$

so that

$$\hat{H} = \frac{\gamma}{(\gamma-1)\bar{\rho}}\hat{p} - \frac{C_p\bar{T}}{\bar{\rho}}\hat{\rho} + \bar{u}\hat{u}. \tag{9}$$

With the base flow solutions and the wave decomposition in Eqs. (2), the stability of the perturbation flow system is solved as an eigenvalue problem of the form:

$$\mathcal{A}(\bar{\mathbf{q}}, \omega)\mathbf{x} = 0. \tag{10}$$

The elements of the vector $\mathbf{x}$ are the decoupled wave amplitudes A_{+j}, A_{-j}, A_{ej} $(j = 1, 2, 3)$ plus the heat release rate fluctuation $\hat{Q}$; $\mathcal{A}$ is the coefficient matrix, as outlined below:

$$\begin{bmatrix} \text{Heat release model (Eq. (5))} \\ \text{Mass conservation equation at } x = l_1 \text{ (Eq. (3)(a))} \\ \text{Isentropic condition at } x = l_1 \text{ (Eq. (3)(b))} \\ \text{Energy conservation equation at } x = l_1 \text{ (Eq. (3)(c))} \\ \text{Mass conservation equation at } x = l_2 \text{ (Eq. (4)(a))} \\ \text{Linear momentum conservation at } x = l_2 \text{ (Eq. (4)(b))} \\ \text{Energy conservation equation at } x = l_2 \text{ (Eq. (4)(c))} \\ \text{Choked inlet condition (Eq. (6)(a))} \\ \text{Isentropic inlet condition (Eq. (6)(b))} \\ \text{Open outlet condition (Eq. (7))} \end{bmatrix} \begin{bmatrix} A_{+1} \\ A_{-1} \\ A_{e1} \\ A_{+2} \\ A_{-2} \\ A_{e2} \\ A_{+3} \\ A_{-3} \\ A_{e3} \\ \hat{Q} \end{bmatrix} = 0. \tag{11}$$

The non-zero elements of the matrix $\mathcal{A}$ are given in Supplementary Material Part B. The nonlinear eigenvalue problem is solved by the inverse iteration algorithm [37]; an advantage of this approach is that for each eigenmode, the left and right eigenvectors are simultaneously obtained. Any complex ω that gives zero determinant of $\mathcal{A}$ is an eigenvalue of the direct system, and the corresponding vector $\mathbf{x}$ is an eigenvector.

The spectrum is formed by ten eigenmodes, shown in Fig. 2. The spectrum shows the trajectories of eigenvalues when the coefficient κ varies. The unsteady flame position is fixed at $x = 1.7345$ m. The comparison of the eigenvalues and the trajectories shows that the frequencies match quite closely those found by Dowling and Stow [35], whereas the growth rates do not. We also observe that both sets of results yield the same sign of the growth rates for nine modes out of ten, when $\kappa = 1$.

The mode shapes of the perturbation variables can be reconstructed from the eigenvector by the use of Eqs. (2). The absolute values of the resonant pressure fluctuations, in the presence of unsteady heat release, are compared with the literature results in Fig. 3. The eigenvalues and the mode shapes of the modes are found to differ mildly from the results of the literature. This could stem from differences in the values of the base flow variables, values not given in the paper by Dowling and Stow [35]. This points to possible uncertainties in the base flow, affecting the amplitude of the perturbations and the complex eigenvalues.

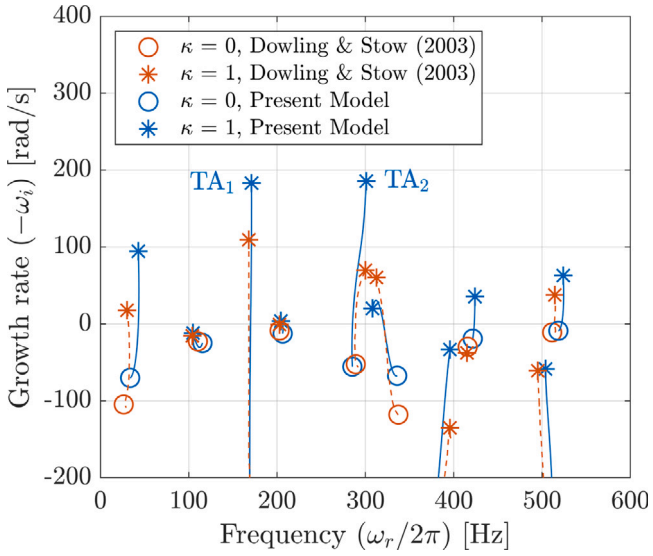

Fig. 2. Comparison of the eigenvalue trajectories against literature results [35], with varying κ, from $\kappa = 0$ (no unsteady heat release at the flame) to $\kappa = 1$. The solid blue lines represent the trajectories of the present model; the dashed red lines represent the trajectories reported in Dowling and Stow [35]. The two most unstable eigenmodes are labeled as TA_1 and TA_2.

3. Uncertainty in base flow parameters

Our first goal is to identify a possible source of discrepancy in the eigenvalues between our results and those in Ref. [35]. We thus employ the adjoint base-state sensitivity analysis to quantify how eigenvalues are affected by small arbitrary variations in base flow variables $\bar{\mathbf{q}}$. The approach used here is similar to the base state sensitivity study carried out by Aguilar et al. [25] and Juniper [30]. However, the purposes are different. The authors above have calculated the effect of system parameters, such as heat release model time delays and reflection coefficients, with the goal of optimizing the system. Here, we aim to evaluate the sensitivity of generic modifications to base flow quantities. In a real physical system, generic base flow modifications can stem from uncertainties in experimental measurements or in numerical computations.

3.1. Base-state sensitivity analysis

Introducing a small deviation $\delta\bar{\mathbf{q}}$ of base flow into the direct system, Eq. (10), causes variations in both eigenfrequency and eigenvector, so that, upon linearization, we have

$$\delta\mathcal{A}\,\mathbf{x} + \mathcal{A}\,\delta\mathbf{x} = 0, \tag{12}$$

with

$$\delta\mathcal{A} = \frac{\partial\mathcal{A}(\bar{\mathbf{q}}, \omega)}{\partial\bar{q}}\,\delta\bar{q} + \frac{\partial\mathcal{A}(\bar{\mathbf{q}}, \omega)}{\partial\omega}\,\delta\omega, \tag{13}$$

where $\bar{q}$ denotes a component of the vector $\bar{\mathbf{q}}$, and a sum over all the components is tacitly assumed.

Left-multiplying Eq. (12) by the adjoint eigenvector, $\mathbf{y}^\dagger$, solution of

$$\mathcal{A}^*(\bar{\mathbf{q}}, \omega)\,\mathbf{y}^\dagger = 0, \tag{14}$$

with $*$ denoting conjugate transpose, we have:

$$\mathbf{y}^{\dagger *}\frac{\partial\mathcal{A}(\bar{\mathbf{q}}, \omega)}{\partial\bar{q}}\,\mathbf{x}\,\delta\bar{q} + \mathbf{y}^{\dagger *}\frac{\partial\mathcal{A}(\bar{\mathbf{q}}, \omega)}{\partial\omega}\,\mathbf{x}\,\delta\omega + \mathbf{y}^{\dagger *}\mathcal{A}(\bar{\mathbf{q}}, \omega)\delta\mathbf{x} = 0, \tag{15}$$

with the last term on the left-hand-side equal to zero by virtue of Eq. (14).

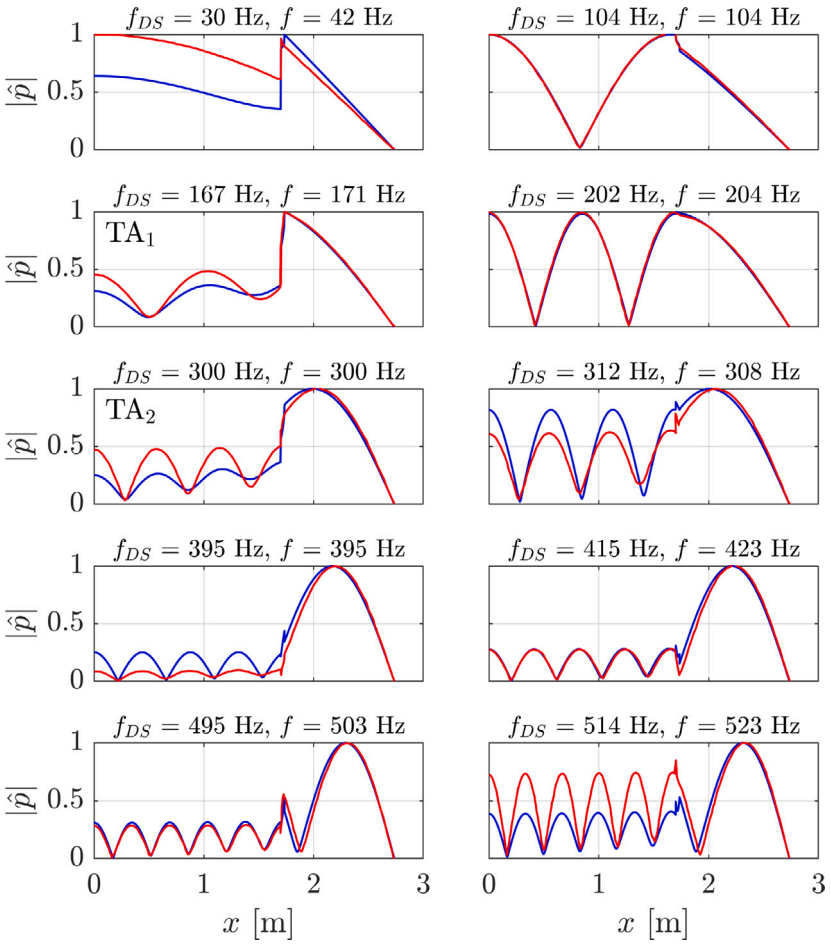

Fig. 3. Shapes of the pressure fluctuation eigenmodes (normalized with the respective maximum amplitudes), in the case of heat release located at x = 1.7345 m. Above each individual frame, the oscillation frequency computed by Dowling and Stow [35] is indicated as f_{DS}, while the value found here is denoted simply by f. Red curves: mode shapes from the literature; blue curves: mode shapes predicted by the present study. The two most unstable modes are labeled TA$_1$ and TA$_2$ within the appropriate frames. (For interpretation of the references to color in this figure legend, the reader is referred to the web version of this article.)

The eigenvalue drift due to a generic base flow modification can thus be written as

$$\delta\omega = S_{\bar{q}}\,\delta\bar{q}, \tag{16}$$

with the sensitivity defined, for each component of the vector $\bar{\mathbf{q}}$, by:

$$S_{\bar{q}} = -\frac{\mathbf{y}^{\dagger *}\dfrac{\partial \mathcal{A}(\bar{\mathbf{q}},\omega)}{\partial \bar{q}}\mathbf{x}}{\mathbf{y}^{\dagger *}\dfrac{\partial \mathcal{A}(\bar{\mathbf{q}},\omega)}{\partial \omega}\mathbf{x}}. \tag{17}$$

3.2. Effects of fractional change of base flow on eigenvalues

We evaluate the variation of any eigenvalue due to a fractional change in the base flow parameters, which can be expressed as

$$\delta\omega = S_{\bar{q}\%}\,\frac{\delta\bar{q}}{\bar{q}}, \tag{18}$$

with the complex, scaled sensitivities defined by

$$S_{\bar{q}\%} = S_{\bar{q}}\,\bar{q}. \tag{19}$$

These scaled sensitivities represent the response of the given eigenvalue to a percentage change in the respective base flow parameters.

Figs. 4 and 6 illustrate the sensitivities of complex eigenvalues to uncertainties in base flow parameters $\bar{\mathbf{q}}$ for the two most unstable modes, TA$_1$ and TA$_2$, with oscillation frequencies of 171 Hz and 300 Hz, respectively. We choose these two eigenmodes because they are the two most unstable modes, and they show large discrepancies in growth rates in the eigenspectrum when compared to the reference results. We also examine how the sensitivities change with varying flame positions (l_2) from 1.7 m to 1.8 m, corresponding to a premixer length, L_2, varying from 0 to 0.1 m.

The sensitivities to modifications of mean pressure and mean density in the combustion chamber ($\bar{\rho}_3$ and $\bar{p}_3$) are zero, as matrix $\mathcal{A}$ does not depend on them. The sensitivity results have been validated against gradients calculated using the finite difference approach, showing excellent agreement. We also conducted a Taylor test to perform a debugging check for adjoint codes: if the small deviation in the base flow quantity is ϵ to calculate the sensitivity with the first-order accurate finite difference approach, then the difference of the eigenvalue drift from that obtained with the adjoint approach ($|\delta\omega_{FD} - \delta\omega_{AD}|$) must increase in proportion to ϵ^2 [20,30]. We show in Fig. 5 an example of changing base flow parameter $\bar{u}_1$. It plots the eigenvalue drift difference for all eigenmodes against ϵ^2 and shows that it is indeed a straight line through the origin.

Our findings indicate that for both eigenmodes TA$_1$ and TA$_2$, the relative difference in oscillation frequencies resulting from base-flow modifications are generally negligible and significantly less pronounced than the relative difference in growth rates. As shown in Fig. 2, the growth rates of modes TA$_1$ and TA$_2$ are overestimated by up to approximately 100 rad/s when compared to Dowling and Stow [35]. However, comparing oscillation frequencies a good agreement can be noticed; our uncertainty calculations confirm this observation.

Among the eleven different base flow modifications considered independently, the effect of mean flow velocity variations in the plenum

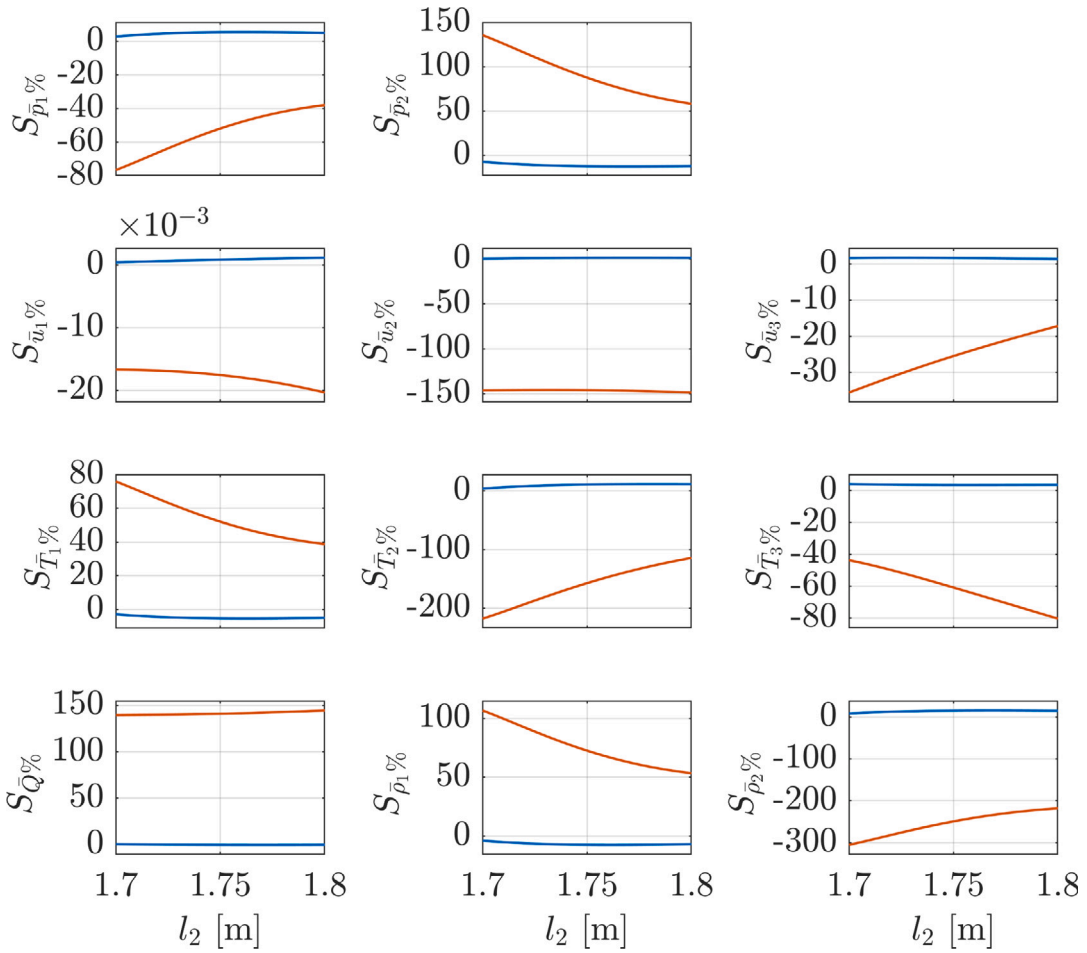

Fig. 4. Sensitivity to uncertainties in different base flow variables for eigenmode TA_1, as a function of the position l_2 of the compact flame. Blue curves: sensitivity of oscillation frequency ($\omega_r/(2\pi)$ [Hz]). Red curves: sensitivity of growth rate ($-\omega_i$ [rad/s]). (For interpretation of the references to color in this figure legend, the reader is referred to the web version of this article.)

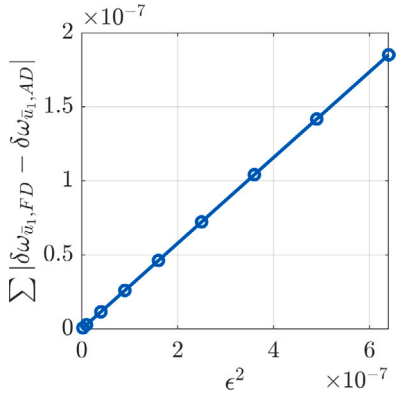

Fig. 5. The difference between the eigenvalue drift of all eigenmodes, calculated from a first-order finite difference method with step size ϵ (FD) and an adjoint approach (AD), for changing base-state parameter $\bar{u}_1$.

is the least significant. A change of 1% in $\bar{u}_1$ leads to a deviation below 0.0204 rad/s in growth rate and below 0.0011 Hz in oscillation frequencies for mode TA_1 for whatever value of l_2 in the range considered; for mode TA_2, a change of 1% in $\bar{u}_1$ leads to a maximum deviation in oscillation frequency of 0.0258 Hz, and in growth rate of 0.0281 rad/s. On the other hand, uncertainties in the mean density in the premixer section have the most profound effect on the linear growth rates for both eigenmodes. A 1% under-estimation of $\bar{\rho}_2$ yields an increase in growth rate of up to 300 rad/s for mode TA_1 and up to 600 rad/s for mode TA_2. The results reported also show that extending the length of the premixer section, L_2, helps reducing the influence of $\bar{\rho}_1$ and $\bar{\rho}_2$ in altering the eigenvalues.

The differences in complex eigenvalues between the present results and those from the literature stem from the combined effect of all base flow uncertainties. The sensitivities displayed in Figs. 4 and 6 give an immediate response for each individual effect; it is the base flow variables in the premixer ($\bar{u}_2, \bar{p}_2, \bar{T}_2, \bar{\rho}_2, \bar{Q}$) which hold the most profound influence. This is due to the fact that these parameters directly affect the flame transfer function, which couples the flow in the premixer with the unsteady heat release. The analysis just presented, thus, furnishes indications of where flow control efforts could be directed.

4. Structural sensitivity to steady feedback forcings

We now assume a general linear feedback forcing acting on the steady base-flow equations, and evaluate the corresponding eigenvalue drift, $\delta\omega$. Differently from the previous section, the base flow variation depends on a particular choice of steady feedback process. In the previous section, we have derived the eigenvalue drift due to arbitrary variations of the base flow. Now, we show the expression of the eigenvalue drift caused by a particular feedback forcing in base flow [18].

The base flow system in compact form is

$$\mathbf{B}(\bar{\mathbf{q}}) = 0. \tag{20}$$

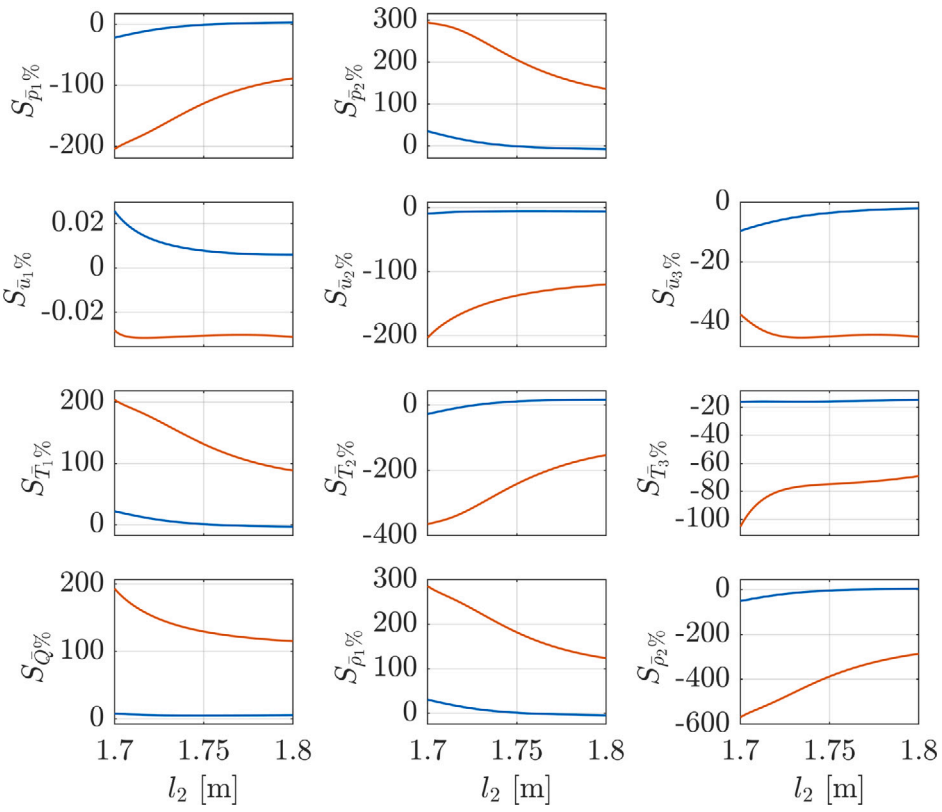

Fig. 6. Same as Fig. 4 for eigenmode TA_2.

Let us assume that a small term $\delta\mathbf{H}_B(\bar{\mathbf{q}})$ forces the system, so that the mean flow is perturbed by $\delta\bar{\mathbf{q}}$, i.e. $\mathbf{B}(\bar{\mathbf{q}}+\delta\bar{\mathbf{q}}) = \delta\mathbf{H}_B(\bar{\mathbf{q}}+\delta\bar{\mathbf{q}})$. Linearization yields

$$\frac{\partial\mathbf{B}(\bar{\mathbf{q}})}{\partial\bar{q}}\,\delta\bar{q} = \delta\mathbf{H}_B(\bar{\mathbf{q}}). \tag{21}$$

Here, again, summation is tacitly implied on the left-hand-side of the equation over all the elements of the vector $\bar{\mathbf{q}}$. Since the base flow is bounded only by jump conditions and boundary conditions, the feedback source term is introduced at the duct intersections, where jump conditions hold, of the form

$$\delta\mathbf{H}_B(\bar{\mathbf{q}}) = \delta\mathbf{H}_{B0}\,\bar{\mathbf{q}} \tag{22}$$

where $\delta\mathbf{H}_{B0}$ is the following coupling coefficient vector,

$$\delta\mathbf{H}_{B0} = [0,0,0,\delta\mathcal{H}_{M1},\delta\mathcal{H}_{M2},\delta\mathcal{H}_{H1},\delta\mathcal{H}_{H2},0,0,0,0,0,0], \tag{23}$$

characterizing feedback mass blowing/suction and feedback heating/cooling mechanisms proportional to the upstream mass flow rate ($\bar{m}$) and total enthalpy($\bar{m}\bar{H}$), respectively.

We now introduce the test variable, $\mathbf{b}^\dagger$, and left-multiply it by Eq. (21); by summing Eq. (15) it is found:

$$\mathbf{b}^{\dagger *}\frac{\partial\mathbf{B}(\bar{\mathbf{q}})}{\partial\bar{q}}\,\delta\bar{q} + \mathbf{y}^{\dagger *}\frac{\partial\mathcal{A}(\bar{\mathbf{q}},\omega)}{\partial\bar{q}}\,\mathbf{x}\,\delta\bar{q} + \mathbf{y}^{\dagger *}\frac{\partial\mathcal{A}(\bar{\mathbf{q}},\omega)}{\partial\omega}\,\mathbf{x}\,\delta\omega = \mathbf{b}^{\dagger *}\delta\mathbf{H}_{B0}\bar{\mathbf{q}}. \tag{24}$$

The adjoint base flow system (given in full form in Supplementary Material Part C) can be formally written as

$$\mathbf{b}^{\dagger *}\frac{\partial\mathbf{B}(\bar{\mathbf{q}})}{\partial\bar{q}} = -\mathbf{y}^{\dagger *}\frac{\partial\mathcal{A}(\bar{\mathbf{q}},\omega)}{\partial\bar{q}}\mathbf{x}. \tag{25}$$

Then, the eigenvalue drift stems naturally from the identity

$$\delta\omega = \mathcal{S}_{\mathbf{H}_{B0}}\,\delta\mathbf{H}_{B0}, \tag{26}$$

where the sensitivity of the eigenvalue to a structural forcing at the base flow level is defined by:

$$\mathcal{S}_{\mathbf{H}_{B0}} = \frac{\mathbf{b}^{\dagger *}\,\bar{\mathbf{q}}}{\mathbf{y}^{\dagger *}\dfrac{\partial\mathcal{A}(\bar{\mathbf{q}},\omega)}{\partial\omega}\,\mathbf{x}}. \tag{27}$$

The structural sensitivity to the feedback forcing at the base flow level for eigenmodes TA_1 and TA_2 is now examined. Two types of feedback sources are considered at the combustor intersections: steady mass blowing or suction, and steady heating or cooling. The corresponding equations are:

$$\bar{\rho}_1\bar{u}_1a_1 - \bar{\rho}_2\bar{u}_2a_2 = \delta\mathcal{H}_{M1}\,\bar{\dot{m}}, \tag{28a}$$

$$\bar{\rho}_2\bar{u}_2a_2 - \bar{\rho}_3\bar{u}_3a_3 = \delta\mathcal{H}_{M2}\,\bar{\dot{m}}, \tag{28b}$$

$$\bar{\rho}_1\bar{u}_1a_1\bar{H}_1 - \bar{\rho}_2\bar{u}_2a_2\bar{H}_2 = \delta\mathcal{H}_{H1}\,\bar{\dot{m}}\,\bar{H}_1, \tag{28c}$$

$$\bar{\rho}_2\bar{u}_2a_2\bar{H}_2 + a_3\bar{Q} - \bar{\rho}_3\bar{u}_3a_3\bar{H}_3 = \delta\mathcal{H}_{H2}\,\bar{\dot{m}}\,\bar{H}_2. \tag{28d}$$

Figs. 7 and 8 show the sensitivities of angular frequency (blue curves) and growth rate (red curves) to steady structural feedback for the two unstable eigenmodes, TA_1 and TA_2, respectively. The sensitivities are evaluated with l_2 ranging from 1.7 m to 1.8 m.[1] The sensitivity results reveal that a small, steady mass suction or the introduction of a steady heat release at the intersections would reduce the growth rate and, therefore, stabilize the eigenmodes. The former steady mechanism is achievable with regulated valves, and the latter one can be obtained with heating coils placed at the duct intersections [31]. For both eigenmodes, sensitivities vary significantly with the length of the premixer, highlighting the fact that a stabilizing or destabilizing geometric

[1] The results have been validated with the gradient calculated by the finite difference approach with percentage differences less than $\mathcal{O}(10^{-3})$. An example of comparison between adjoint and finite difference gradient evaluation will be shown in the next section.

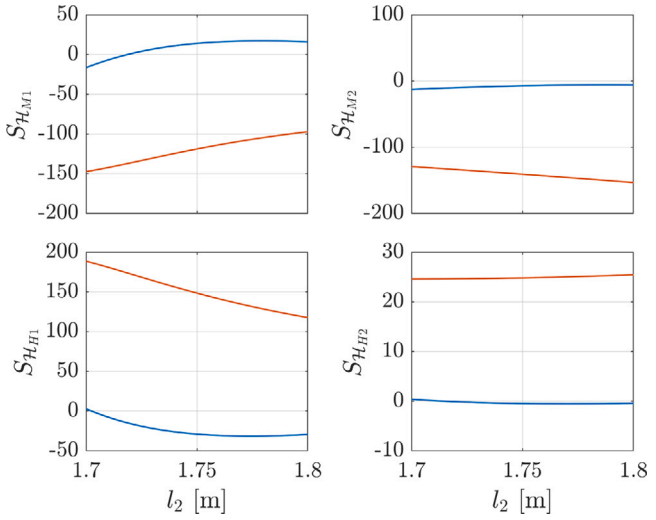

Fig. 7. Sensitivity of ω to structural feedback in base flow level, for the eigenmode TA_1, $f = 171$ [Hz], with the variation of the compact flame position (l_2). Blue curves: sensitivity of angular eigenfrequencies (ω_r); Red curves: sensitivity of growth rate ($-\omega_i$). (For interpretation of the references to color in this figure legend, the reader is referred to the web version of this article.)

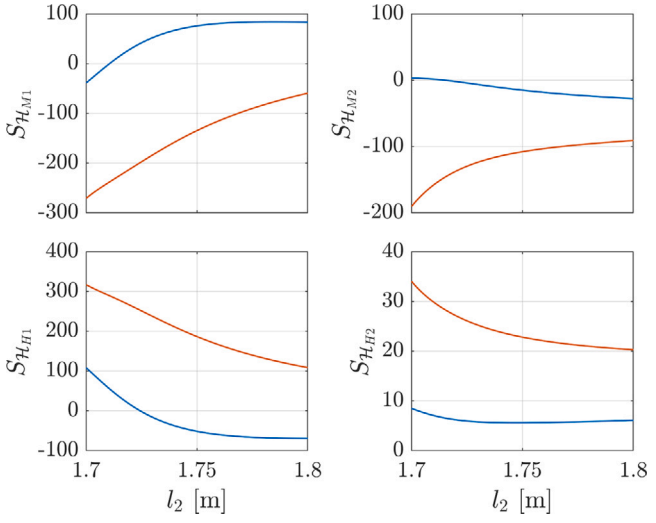

Fig. 8. Same as Fig. 7 for mode TA_2, $f = 300$ [Hz]. (For interpretation of the references to color in this figure legend, the reader is referred to the web version of this article.)

configuration for mode TA_1 might produce the opposite effect for TA_2. The results confirm our observations in the previous section: variations of base flow parameters in the premixer, produced at the 1–2 interface and propagating downstream, resulting in the most significant changes in the two eigenvalues examined.

5. Sensitivity to structural perturbations

We now evaluate the eigenvalue response to a localized feedback source acting on the differential equations (1) for the perturbations.

5.1. Derivation of structural sensitivity

In some previous literature (e.g. [25]), the structural sensitivity is derived based on a Lagrange multiplier framework. In the present work, the derivation of the structural sensitivity follows Luchini et al. [19] and Pralits et al. [18] with a method based on the Lagrange identity, also used by Magri and Juniper [38]. Note that the choice of the derivation method does not lead to different results.

Table 2
Units of the feedback coupling coefficients.

$\delta\mathcal{M}_\rho$	$\delta\mathcal{M}_u$	$\delta\mathcal{M}_p$	$\delta\mathcal{F}_\rho$	$\delta\mathcal{F}_u$	$\delta\mathcal{F}_p$	$\delta\mathcal{Q}_\rho$	$\delta\mathcal{Q}_u$	$\delta\mathcal{Q}_p$
s m^{-1}	kg m^{-3}	m s^{-1}	1	kg m^{-2} s^{-1}	m^2 s^{-2}	m s^{-1}	Pa	m^2 s^{-2}

The derivation starts with the direct system in compact form:

$$\begin{aligned}\mathcal{N}(\omega,\bar{\mathbf{q}})\,\hat{\mathbf{q}} &= 0,\\ \mathcal{J}(\omega,\bar{\mathbf{q}},\hat{\mathbf{q}}) &= 0,\end{aligned} \tag{29}$$

with perturbation variable vector $\hat{\mathbf{q}} = (\hat{\rho},\hat{u},\hat{p})$; the equation $\mathcal{J}(\omega,\bar{\mathbf{q}},\hat{\mathbf{q}}) = 0$ represents the jump conditions, Eqs. (3)–(4), holding at the ducts' intersections, and $\mathcal{N}(\omega,\bar{\mathbf{q}})$ is the differential operator matrix defined by:

$$\mathcal{N}(\omega,\bar{\mathbf{q}}) = \begin{bmatrix} \mathrm{i}\omega + \bar{u}\dfrac{\mathrm{d}}{\mathrm{d}x} & \bar{\rho}\dfrac{\mathrm{d}}{\mathrm{d}x} & 0 \\ 0 & \mathrm{i}\omega\bar{\rho} + \bar{\rho}\bar{u}\dfrac{\mathrm{d}}{\mathrm{d}x} & \dfrac{\mathrm{d}}{\mathrm{d}x} \\ 0 & \gamma\bar{p}\dfrac{\mathrm{d}}{\mathrm{d}x} & \mathrm{i}\omega + \bar{u}\dfrac{\mathrm{d}}{\mathrm{d}x} \end{bmatrix}. \tag{30}$$

Now, we introduce a small structural perturbation localized in space (*via* a Dirac delta function $\delta(x-x_0)$, $x_0 \neq l_1$ and $x_0 \neq l_2$), proportional to a local fluctuating quantity $\hat{\mathbf{q}}$, i.e.

$$\delta\mathbf{H}(\hat{\mathbf{q}}) = \delta\mathbf{H}_0\,\hat{\mathbf{q}}\,\delta(x-x_0), \tag{31}$$

where $\delta\mathbf{H}_0$ is the coupling coefficient matrix

$$\delta\mathbf{H}_0 = \begin{bmatrix} \delta\mathcal{M}_\rho & \delta\mathcal{M}_u & \delta\mathcal{M}_p \\ \delta\mathcal{F}_\rho & \delta\mathcal{F}_u & \delta\mathcal{F}_p \\ \delta(\mathcal{Q}_\rho + \bar{c}^2\mathcal{M}_\rho) & \delta(\mathcal{Q}_u + \bar{c}^2\mathcal{M}_u) & \delta(\mathcal{Q}_p + \bar{c}^2\mathcal{M}_p) \end{bmatrix}, \tag{32}$$

which encompasses nine different feedback mechanisms, $\mathcal{M}$, $\mathcal{F}$, and $\mathcal{Q}$ denote forcing on the mass, momentum, and energy conservation equation, respectively. For the forcing of the energy conservation equation, the feedback coupling coefficient $\delta(\mathcal{Q}_q + \bar{c}^2\mathcal{M}_q)$ includes an additional term due to the derivation process involving the mass conservation equation. The units of these coupling coefficients are listed in Table 2.

Paying attention to not confuse the Dirac delta, $\delta(x-x_0)$, with the δ used to denote small variations, we express the perturbed eigenvalue problem to first order as

$$\delta\mathcal{N}\,\hat{\mathbf{q}} + \mathcal{N}\,\delta\hat{\mathbf{q}} = \delta\mathbf{H}_0\,\hat{\mathbf{q}}\,\delta(x-x_0), \tag{33a}$$

$$\delta\mathcal{J} = 0, \tag{33b}$$

with the boundary conditions defined as Eqs. (6)–(7). Fixing the base flow, the above takes the form:

$$\frac{\partial\mathcal{N}(\omega,\bar{\mathbf{q}})}{\partial\omega}\delta\omega\,\hat{\mathbf{q}} + \mathcal{N}(\omega,\bar{\mathbf{q}})\,\delta\hat{\mathbf{q}} = \delta\mathbf{H}_0\,\hat{\mathbf{q}}\,\delta(x-x_0), \tag{34a}$$

$$\frac{\partial\mathcal{J}(\omega,\bar{\mathbf{q}},\hat{\mathbf{q}})}{\partial\omega}\delta\omega + \frac{\partial\mathcal{J}(\omega,\bar{\mathbf{q}},\hat{\mathbf{q}})}{\partial\hat{q}}\delta\hat{q} = 0. \tag{34b}$$

We left-multiply by the test variable, $\hat{\mathbf{q}}^\dagger$, and integrate in space, i.e.

$$\begin{aligned}&\int\left[\hat{\mathbf{q}}^{\dagger *}\mathcal{N}(\omega,\bar{\mathbf{q}})\,\delta\hat{\mathbf{q}}\right]\mathrm{d}x + \int\left[\hat{\mathbf{q}}^{\dagger *}\frac{\partial\mathcal{N}(\omega,\bar{\mathbf{q}})}{\partial\omega}\delta\omega\,\hat{\mathbf{q}}\right]\mathrm{d}x + \\ &+\hat{\mathbf{f}}^{\dagger *}\left[\frac{\partial\mathcal{J}(\omega,\bar{\mathbf{q}},\hat{\mathbf{q}})}{\partial\omega}\delta\omega + \frac{\partial\mathcal{J}(\omega,\bar{\mathbf{q}},\hat{\mathbf{q}})}{\partial\hat{q}}\delta\hat{q}\right] = \int\hat{\mathbf{q}}^{\dagger *}\delta\mathbf{H}_0\,\hat{\mathbf{q}}\,\delta(x-x_0)\mathrm{d}x.\end{aligned} \tag{35}$$

We apply integration by parts, for the first term on the left-hand-side to yield the adjoint equation:

$$\mathcal{N}^*(\omega,\bar{\mathbf{q}})\,\hat{\mathbf{q}}^\dagger = 0. \tag{36}$$

The boundary terms generated from integration by parts plus the term $\hat{\mathbf{f}}^{\dagger *}\dfrac{\partial\mathcal{J}(\omega,\bar{\mathbf{q}},\hat{\mathbf{q}})}{\partial\hat{q}}\delta\hat{q}$ give the boundary and jump conditions of the adjoint system. The detailed equations of the adjoint disturbance system are

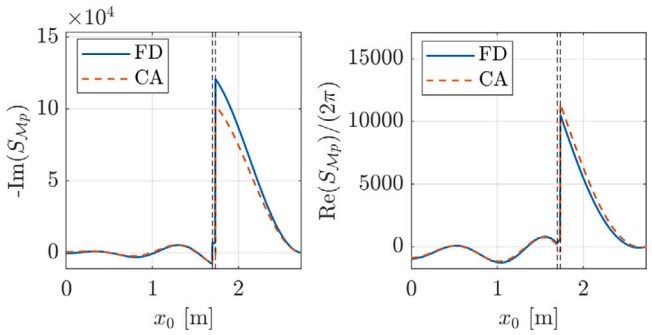

Fig. 9. Validation with first-order finite difference approach, for mass feedback forcing proportional to pressure oscillations, with $\delta\mathcal{M}_p = 1\times10^{-7}$. The structural sensitivity are shown for the least stable eigenmode TA_1 for (a) growth rate and (b) oscillation frequency. The dashed lines represent the positions of the boundaries of each duct. FD: finite difference approach; CA: continuous adjoint approach.

listed in Supplementary Material Part D. The eigenvalue drift due to a localized structural perturbation can finally be written as

$$\delta\omega = S_{\mathbf{H}_0}\,\delta\mathbf{H}_0, \tag{37}$$

with the sensitivity function defined by:

$$S_{\mathbf{H}_0} = \frac{\hat{\mathbf{q}}^{\dagger *}(x_0)\,\hat{\mathbf{q}}(x_0)}{\int\left[\hat{\mathbf{q}}^{\dagger *}\dfrac{\partial\mathcal{N}(\omega,\bar{\mathbf{q}})}{\partial\omega}\hat{\mathbf{q}}\right]\mathrm{d}x + \hat{\mathbf{f}}^{\dagger *}\dfrac{\partial\mathcal{J}(\omega,\bar{\mathbf{q}},\hat{\mathbf{q}})}{\partial\omega}}. \tag{38}$$

5.2. Validation with finite difference approach

The sensitivity results are validated with the gradient calculated with a first-order finite difference approach. With the finite difference approach, a set of jump conditions at position x_0 is added to the system:

$$(\bar{u}\hat{\rho}+\bar{\rho}\hat{u})|_{x_{0-}}^{x_{0+}} = \delta\mathcal{M}_q\hat{q}(x_0), \tag{39a}$$

$$(\bar{u}\bar{\rho}\hat{u}+\hat{p})|_{x_{0-}}^{x_{0+}} = \delta\mathcal{F}_q\hat{q}(x_0), \tag{39b}$$

$$(\bar{u}\hat{p}+\gamma\bar{p}\hat{u})|_{x_{0-}}^{x_{0+}} = (\delta\mathcal{Q}_q+\bar{c}^2\delta\mathcal{M}_q)\hat{q}(x_0). \tag{39c}$$

The eigenvalue change due to each feedback disturbance can be evaluated individually at each discrete position x_0. Suppose that the length of the combustor is discretized into n points; a first order finite-difference approach requires solving nonlinear eigenvalue problems at each discretized point in the combustor and for each feedback mechanism, hence, a total number of $18n$ times. With the adjoint approach, the sensitivity information is obtained by first solving the direct and adjoint nonlinear eigenvalue problem a single time for each eigenmode. The structural sensitivity, as a function of x_0, is then evaluated n times from the direct and adjoint modes. A sample comparison of results is displayed in Fig. 9, highlighting the good agreement between adjoint sensitivity results and results from the finite-difference approach. A similar agreement is obtained for all other feedback sources. Once the adjoint system is established, the method proposed yields sensitivity information rapidly. On the other hand, deriving adjoint equations requires some effort.

5.3. The structural sensitivity of the most unstable eigenmodes

Figs. 10 and 11 show the structural sensitivity defined by Eq. (38) for the two most unstable eigenmodes, TA_1 and TA_2. We aim to identify possible feedback mechanisms in the perturbation flow that can stabilize the system. The red curves illustrate the structural sensitivity of the growth rate; the blue curves illustrate the structural sensitivity of the oscillation frequency.

The nine feedback mechanisms can be evaluated comparatively; mass forcing proportional to pressure oscillations appears to have a very significant effect on the eigenvalue, for both modes. Such an effect can be generated by a Helmholtz resonator [30,33,39], consisting of a cavity connected to a narrow neck or a small opening. When acoustic waves reach the resonator, the air in the neck oscillates in and out of the cavity, inducing mass flow disturbances. Such disturbances compress the air in the cavity, exciting the resonant frequency of the Helmholtz resonator. When the pressure oscillations in the combustion system match the resonant frequency of the resonator, the air in the neck oscillates, converting the acoustic energy into kinetic energy and subsequently dissipating it into heat, thereby reducing the amplitude of the pressure oscillations. Focusing on the sensitivity of growth rates, it can be seen that a strong stabilizing effect for the leading unstable mode can be achieved by putting a Helmholtz resonator in the premixer or in the combustion section. In practice, the resonator should be tuned so that the phase between the mass disturbances and the pressure oscillations favors suppression of the instability [31].

Reducing mass flow rate disturbances with a feedback term acting on the local velocity oscillations at the inlet of the premixer or adding a force proportional to the local pressure oscillations at the outlet of the premixer also help stabilizing the critical unstable eigenmodes. Active flow control devices are available to achieve these feedback mechanisms, with actuators and sensors specifically designed, such as synthetic jets [40] and loudspeaker–microphone devices [41]. The structural sensitivity analysis also reveals that introducing a feedback forcing proportional to the unsteady heat release has a minor effect on the system's stability.

6. Summary and conclusions

In this study, an adjoint sensitivity analysis was applied to a prototypical thermoacoustic system. We analyzed the eigenvalues of the system and identified the most unstable resonant modes. By focusing on the two least stable modes, we investigated three types of sensitivities, using the adjoint method.

First, we compared our eigenvalue spectra with those in the literature and found discrepancies, mainly in the growth rates of the resonant disturbances. Since we believe that these discrepancies might be due to inconsistencies in base flow parameters, we evaluated the effect of generic base-flow modifications on the eigenvalues; our findings indicated that the mean densities of the cold gaseous fuel within the premixing duct had the most significant impact on complex eigenvalues, particularly on altering growth rates. Additionally, we demonstrated that extending the length of the premixer duct significantly reduces the sensitivity of eigenvalues to mean density variations.

Then, we examined the use of steady forcing terms on the base flow equations to stabilize critical eigenmodes. The sensitivity analysis indicated that steady mass reduction or introducing steady heat release at both ducts' intersections can stabilize the unstable eigenmodes. The stabilizing effect is more significant when the premixer duct is relatively short, i.e., the flame position moves upstream.

Finally, we assessed the sensitivities of the two most unstable eigenmodes to feedback disturbances. We found that mass fluctuation feedback proportional to local pressure perturbations, achievable through a Helmholtz resonator placed in the premixer and/or the combustion chamber, can have a strong effect in stabilizing the instabilities. The structural sensitivity analysis also revealed that active control approaches, such as reduction in mass flow rate fluctuations, proportional to velocity disturbances, and the imposition of an external force, proportional to pressure perturbations, are viable options to modify the system's stability.

In conclusion, even though our model problem is not very high dimensional, our findings highlight the effectiveness of adjoint-based sensitivity analysis in explaining and quantifying uncertainties in a thermoacoustic system, and in suggesting effective control strategies for mitigating temporally growing modes.

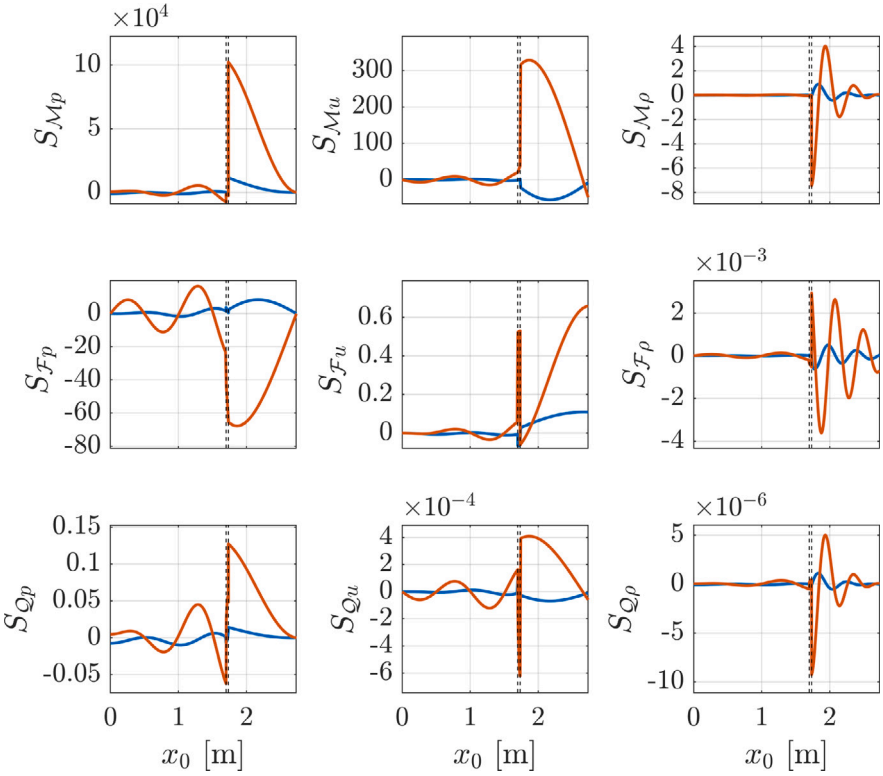

Fig. 10. The structural sensitivity of eigenvalue to nine different feedback mechanisms placed at position x_0. Eigenmode TA_1, $f = 171$ [Hz]. Blue curves: structural sensitivity of the oscillation frequency ($\omega_r/2\pi$ [Hz]); red curves: structural sensitivity of the growth rate ($-\omega_i$ [rad/s]). (For interpretation of the references to color in this figure legend, the reader is referred to the web version of this article.)

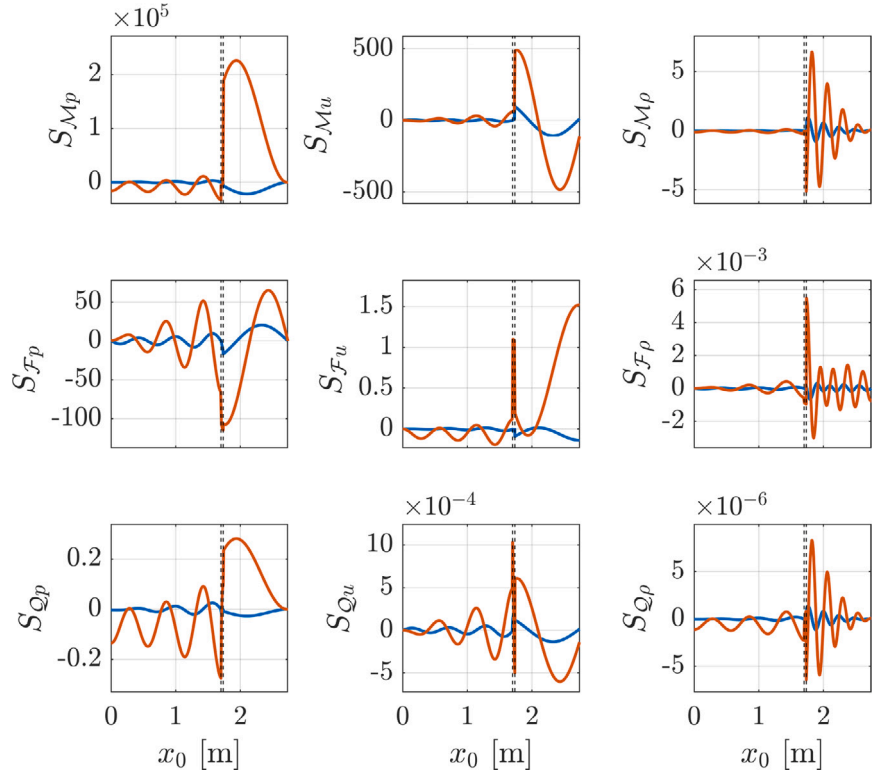

Fig. 11. Same as Fig. 10 for eigenmode TA_2. (For interpretation of the references to color in this figure legend, the reader is referred to the web version of this article.)

CRediT authorship contribution statement

Jiasen Wei: Writing – original draft, Visualization, Validation, Software, Methodology, Investigation, Formal analysis, Data curation, Conceptualization. **Alessandro Bottaro:** Writing – review & editing, Supervision, Resources, Project administration, Methodology, Funding acquisition, Conceptualization. **Jan O. Pralits:** Writing – review & editing, Supervision, Software, Resources, Methodology, Conceptualization.

Declaration of competing interest

The authors declare that they have no known competing financial interests or personal relationships that could have appeared to influence the work reported in this paper.

Acknowledgments

This work is part of the Marie Skłodowska-Curie Innovative Training Network ***Pollution Know-How and Abatement*** (POLKA). We gratefully acknowledge the financial support from the European Union's Horizon 2020 research and innovation program under the Marie Skłodowska-Curie grant agreement No. 813367.

Appendix A. Supplementary data

Supplementary material related to this article can be found online at https://doi.org/10.1016/j.combustflame.2024.113901.

References

[1] T.C. Lieuwen, V. Yang, Combustion Instabilities in Gas Turbine Engines: Operational Experience, Fundamental Mechanisms, and Modeling, American Institute of Aeronautics and Astronautics, Inc., ISBN: 978-1-56347-669-3, 2005.
[2] F.E.C. Culick, Combustion instabilities in liquid-fuelled propulsion systems – an overview, in: AGARD Conference Proceedings, Vol. 450, 1988, pp. 1–73.
[3] R. Raun, M. Beckstead, J. Finlinson, K. Brooks, A review of Rijke tubes, Rijke burners and related devices, Prog. Energy Combust. Sci. 19 (4) (1993) 313–364.
[4] K. Balasubramanian, R.I. Sujith, Thermoacoustic instability in a Rijke tube: Non-normality and nonlinearity, Phys. Fluids 20 (4) (2008) 044103.
[5] A.P. Dowling, The calculation of thermoacoustic oscillations, J. Sound Vib. 180 (4) (1995) 557–581.
[6] T. Sayadi, V. Le Chenadec, P.J. Schmid, F. Richecoeur, M. Massot, Thermoacoustic instability – a dynamical system and time domain analysis, J. Fluid Mech. 753 (2014) 448–471.
[7] J.W.S.B. Rayleigh, The Theory of Sound: in Two Volumes, Vol. 2, The Macmillan Company, 1896.
[8] L. Crocco, S.I. Cheng, Theory of Combustion Instability in Liquid Propellant Rocket Motors, Butterworths Publications LTD., 88 Kingsway, London, 1956.
[9] F. Schaefer, W. Polifke, Low-order network model of a duct with non-uniform cross-section and varying mean temperature in the presence of mean flow, in: AIAA Propulsion and Energy 2019 Forum, 2019, p. 4376.
[10] S. Evesque, W. Polifke, Low-order acoustic modelling for annular combustors: Validation and inclusion of modal coupling, in: ASME Turbo Expo: Power for Land, Sea, and Air, 2002, pp. 321–331.
[11] G. Ghirardo, C. Di Giovine, J.P. Moeck, M.R. Bothien, Thermoacoustics of can-annular combustors, J. Eng. Gas Turb. Power 141 (1) (2019) 011007.
[12] J.O. Pralits, A. Hanifi, D. Henningson, Adjoint-based optimization of steady suction for disturbance control in incompressible flows, J. Fluid Mech. 467 (2002) 129–161.
[13] P. Luchini, A. Bottaro, Adjoint equations in stability analysis, Annu. Rev. Fluid Mech. 46 (2014) 493–517.
[14] P.J. Schmid, L. Brandt, Analysis of fluid systems: Stability, receptivity, sensitivity, Appl. Mech. Rev. 66 (2) (2014) 024803.
[15] A. Bottaro, P. Corbett, P. Luchini, The effect of base flow variation on flow stability, J. Fluid Mech. 476 (2003) 293–302.
[16] F. Giannetti, P. Luchini, Structural sensitivity of the first instability of the cylinder wake, J. Fluid Mech. 581 (2007) 167–197.
[17] O. Marquet, D. Sipp, L. Jacquin, Sensitivity analysis and passive control of cylinder flow, J. Fluid Mech. 615 (2008) 221–252.
[18] J.O. Pralits, L. Brandt, F. Giannetti, Instability and sensitivity of the flow around a rotating circular cylinder, J. Fluid Mech. 650 (2010) 513–536.
[19] P. Luchini, F. Giannetti, J. Pralits, Structural sensitivity of linear and nonlinear global modes, in: 5th AIAA Theoretical Fluid Mechanics Conference, 2008, pp. 1–19.
[20] M.P. Juniper, R.I. Sujith, Sensitivity and nonlinearity of thermoacoustic oscillations, Annu. Rev. Fluid Mech. 50 (2018) 661–689.
[21] A. Orchini, M.P. Juniper, Linear stability and adjoint sensitivity analysis of thermoacoustic networks with premixed flames, Combust. Flame 165 (2016) 97–108.
[22] L. Magri, Adjoint methods as design tools in thermoacoustics, Appl. Mech. Rev. 71 (2019) 080201.
[23] S. Falco, M.P. Juniper, Shape optimization of thermoacoustic systems using a two-dimensional adjoint Helmholtz solver, J. Eng. Gas Turb. Power 143 (2021) 071025.
[24] J.G. Aguilar, M.P. Juniper, Shape optimization in low-order thermoacoustic networks, in: Proceedings of GPPS Forum 18 Global Power and Propulsion Society, 2018.
[25] J.G. Aguilar, L. Magri, M.P. Juniper, Adjoint-based sensitivity analysis of low-order thermoacoustic networks using a wave-based approach, J. Comput. Phys. 341 (2017) 163–181.
[26] J.G. Aguilar, M.P. Juniper, Thermoacoustic stabilization of a longitudinal combustor using adjoint methods, Phys. Rev. Fluids 5 (2020) 083902.
[27] G.A. Mensah, J.P. Moeck, Acoustic damper placement and tuning for annular combustors: an adjoint-based optimization study, J. Eng. Gas Turb. Power 139 (6) (2017).
[28] L. Magri, M.P. Juniper, J.P. Moeck, Sensitivity of the Rayleigh criterion in thermoacoustics, J. Fluid Mech. 882 (2020) R1.
[29] F. Schäfer, L. Magri, W. Polifke, A hybrid adjoint network model for thermoacoustic optimization, J. Eng. Gas Turb. Power 144 (3) (2022) 031017.
[30] M.P. Juniper, Sensitivity analysis of thermoacoustic instability with adjoint Helmholtz solvers, Phys. Rev. Fluids 3 (11) (2018) 110509.
[31] S. Raghu, K.R. Sreenivasan, Control of acoustically coupled combustion and fluid dynamic instabilities, in: 11th Aeroacoustics Conference, 1987, p. 2690.
[32] A.P. Dowling, A.S. Morgans, Feedback control of combustion oscillations, Annu. Rev. Fluid Mech. 37 (2005) 151–182.
[33] D. Zhao, X.Y. Li, A review of acoustic dampers applied to combustion chambers in aerospace industry, Prog. Aerosp. Sci. 74 (2015) 114–130.
[34] D. Zhao, A.S. Morgans, Tuned passive control of combustion instabilities using multiple Helmholtz resonators, J. Sound Vib. 320 (4–5) (2009) 744–757.
[35] A.P. Dowling, S.R. Stow, Acoustic analysis of gas turbine combustors, J. Propul. Power 19 (5) (2003) 751–764.
[36] S.R. Stow, A.P. Dowling, T.P. Hynes, Reflection of circumferential modes in a choked nozzle, J. Fluid Mech. 467 (2002) 215–239.
[37] D.S. Watkins, Fundamentals of Matrix Computations, second ed., John Wiley & Sons, Inc. New York, 2002.
[38] L. Magri, M.P. Juniper, Sensitivity analysis of a time-delayed thermo-acoustic system via an adjoint-based approach, J. Fluid Mech. 719 (2013) 183–202.
[39] I.D.J. Dupere, A.P. Dowling, The use of Helmholtz resonators in a practical combustor, J. Eng. Gas Turb. Power 127 (2) (2005) 268–275.
[40] K. McManus, U. Vandsburger, C. Bowman, Combustor performance enhancement through direct shear layer excitation, Combust. Flame 82 (1) (1990) 75–92.
[41] A.M. Annaswamy, A.F. Ghoniem, Active control in combustion systems, IEEE Control Syst. Mag. 15 (6) (1995) 49–63.